Dissociative Recombination of Cold HeH$^+$ Ions

Roman Čurík[*]

J. Heyrovský Institute of Physical Chemistry, ASCR, Dolejškova 3, 18223 Prague, Czech Republic

Dávid Hvizdoš

J. Heyrovský Institute of Physical Chemistry, ASCR, Dolejškova 3, 18223 Prague, Czech Republic
and Institute of Theoretical Physics, Faculty of Mathematics and Physics, Charles University in Prague,
V Holešvičkách 2, 180 00 Prague, Czech Republic

Chris H. Greene

Department of Physics and Astronomy, Purdue University, West Lafayette, Indiana 47907, USA
and Purdue Quantum Science and Engineering Institute, Purdue University, West Lafayette, Indiana 47907, USA

The HeH$^+$ cation is the simplest molecular prototype of the indirect dissociative recombination (DR) process that proceeds through electron capture into Rydberg states of the corresponding neutral molecule. This Letter develops the first application of our recently developed energy-dependent frame transformation theory to the indirect DR processes. The theoretical model is based on the multichannel quantum-defect theory with the vibrational basis states computed using exterior complex scaling of the nuclear Hamiltonian. The *ab initio* electronic R-matrix theory is adopted to compute quantum defects as functions of the collision energy and of the internuclear distance. The resulting DR rates are convolved over the beam energy distributions relevant to a recent experiment at the Cryogenic Storage Ring, giving good agreement between the experiment and the theory.

The HeH$^+$ ion, probably the oldest molecule in the Universe, had eluded astrophysical observation for decades. Only very recently, Guesten *et al.* [1] finally reported the detection of HeH$^+$ ions in the nebula NGC 7027. The authors created a simple reaction chain model in which the dominant roles are played by two competing processes: the association (RA) of He$^+$ and H atoms to form HeH$^+$ and the dissociative recombination which destroys the molecule:

$$\text{HeH}^+ + e^- \rightarrow \text{He} + \text{H}. \qquad (1)$$
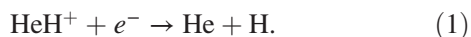
The observed beam brightness of the pure rotational transition $j = 1 \rightarrow 0$ was about $4\times$ higher than the value based on the rate constants for the RA (1.4×10^{-16} cm^3/s) and the DR (3.0×10^{-10} cm^3/s) processes at a kinetic temperature of 10^4 K. This appears to indicate that either the currently known RA rate [2] underestimates the production of HeH$^+$ cations or else the measured DR rate [3] overestimates their destruction rate.

Initial state-specific DR rate coefficients have recently been measured at the Cryogenic Storage Ring (CSR) [4]. The experimental collaboration observed a dramatic decrease of the DR rate at very low collision energies (below 20 meV), far smaller than those observed in previous measurements [3] at room temperature. Such a reduced

destruction rate of the HeH$^+$ ions should be reflected by their higher abundance in cold interstellar environments.

A number of computational methods have been previously applied to study the DR of HeH$^+$. The pioneering work of Guberman [5] was based on the traditional Born-Oppenheimer framework, with the neutral HeH curves coupled to each other by nonadiabatic coupling terms and with rotational effects neglected. All the treatments that followed [6–9] were based on the rovibrational frame transformation combined with multichannel quantum-defect theory (MQDT). They differed in their treatments of the nuclear dynamics and in the accuracy of the quantum-defect matrix $\boldsymbol{\mu}(R)$—a single electronic-structure quantity necessary to carry out these calculations. The most recent calculations by Čurík and Greene [9] exhibit decent agreement with the hot ions experiment of Stromholm *et al.* [3] but the predicted value of the DR rate from the initial $j' = 0$ state at low electron temperatures is about one order of magnitude higher than the values deduced in the recent cryogenic experiment [4].

This Letter introduces a practical application of the reformulated energy-dependent frame transformation theory we have developed [10] for treating vibrational excitation and dissociative recombination processes. The method was derived by the use of a simple 2D model [11] in which the total, electronic and nuclear Hamiltonian was tailored to approximately describe the $^1\Sigma$ ungerade states of

043401-1

H_2. Such a model system can be solved exactly in two dimensions (one electronic and one nuclear coordinate), altogether avoiding the Born-Oppenheimer approximation. Therefore, it can provide an exact benchmark for an approximate theory, such as the frame transformation approach. All the technical details of the method are present in our companion paper [10], while this Letter deals only with the procedural steps relevant for treating electron collisions with HeH^+.

In contrast to the previous DR studies of HeH^+, the present treatment is based on the energy-dependent quantum-defect matrix, approximated throughout this study with a linear energy dependence, as

$$\boldsymbol{\mu}^\Lambda(R, \epsilon) = \boldsymbol{\mu}^\Lambda(R) + \epsilon\boldsymbol{\mu}'^\Lambda(R). \tag{2}$$

Here, ϵ represents the body-frame electron energy, and Λ denotes the projection of the Rydberg electron angular momentum l onto the molecular axis. The accuracy of the approximation (2) is inspected in the Supplemental Material [12].

The quantum-defect matrices have been computed using the diatomic part of the UK Molecular R-matrix Codes [17] with the R-matrix boundary set at $r_0 = 20$ bohr. Bound electrons are described in the Slater-type basis [18] (STO) of triple-zeta quality (denoted as VB2 in Ref. [18]). The angular space of the colliding (or Rydberg) electron is limited by $l_{\max} = 2$ (with $\Lambda_{\max} = 2$), which we previously found [9] to be sufficient when working in the center-of-charge frame of reference.

The zero-energy quantum-defect matrix $\boldsymbol{\mu}^\Lambda(R)$ and the linear coefficient $\boldsymbol{\mu}'^\Lambda(R)$ in Eq. (2) are obtained by carrying out fixed-nuclei scattering calculations for the $e^- + HeH^+$ system, for collision energies $\epsilon_1 = 20$ meV and $\epsilon_2 = 420$ meV, followed by numerical differentiation. The stability of this procedure was checked by changing ϵ_2 to 220 and 620 meV. Upon these changes the matrix $\boldsymbol{\mu}'^\Lambda(R)$ varied only within 1%–2%, while variations of $\boldsymbol{\mu}^\Lambda(R)$ were smaller than 0.2%.

The resulting R dependences of the $\boldsymbol{\mu}^\Lambda(R)$ and $\boldsymbol{\mu}'^\Lambda(R)$ elements are shown in Figs. 1 and 2 for $\Lambda = 0$. While the data shown in Fig. 1 are very similar to the quantum defects published previously [9], the linear energy slope coefficients displayed in Fig. 2 are new. Quantum defects (and their energy dependence) for $\Lambda = 1, 2$ have also been computed and used in the present work. However, since their impact on the final DR rates is minor, they are not shown here.

The rovibrational nuclear basis, serving as channel functions in the MQDT framework, is generated by numerically solving the nuclear Schrödinger equation

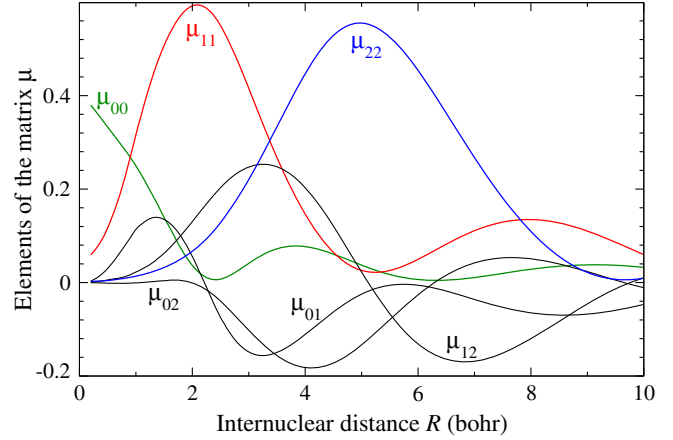$$\left[-\frac{d^2}{dZ^2} + 2MU^+(Z) + \frac{j(j+1)}{Z^2} - K_{\nu j}^2 \right] \phi_{\nu j}(Z) = 0, \tag{3}$$

FIG. 1. Matrix elements of the $\boldsymbol{\mu}(R)$ matrix for $\Lambda = 0$. Indexes of the $\boldsymbol{\mu}(R)$ correspond to the angular momenta of the colliding (or Rydberg) electron.

where $U^+(Z)$ is the ground-state $^1\Sigma_g^+$ potential curve of the target cation and the atom-ion reduced mass $M = 1467.28$ a.u. was taken from Ref. [19]. The nuclear Schrödinger equation (3) is solved on a complex contour Z of the internuclear distances, according to the exterior complex scaling (ECS) technique [20,21]:

$$Z = \begin{cases} R, & \text{for } R \le R_0, \\ R_0 + e^{i\theta}(R - R_0), & \text{for } R_0 < R \le R_m, \end{cases} \tag{4}$$

where R is a real parameter along the complex contour Z, $R_0 = 10$ bohr denotes the bending point, $\theta = 40°$ is the bending angle, and $R_m = 25$ bohr parametrizes the final point Z_m of the complex contour. Boundary conditions for the solutions are $\phi_{\nu j}(0) = \phi_{\nu j}(Z_m) = 0$. An example of the complex eigenmomenta $K_{\nu j}$ spectrum is shown in Fig. 3 for $j = 0$. It is similar to that obtained using the Siegert pseudostate [22,23] spectrum that has been employed in
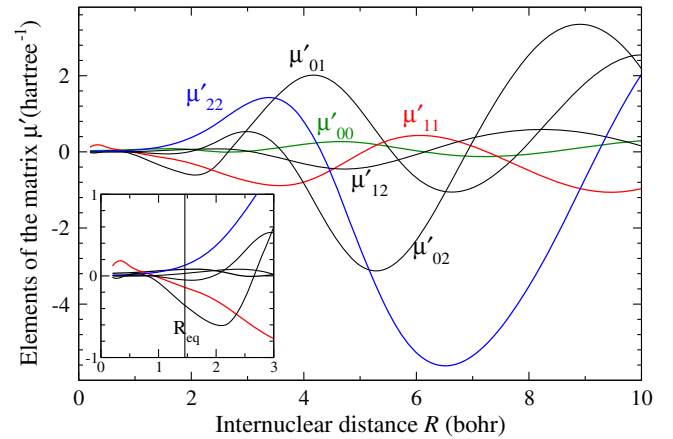

FIG. 2. Matrix elements of the $\boldsymbol{\mu}'(R)$ matrix for $\Lambda = 0$. Indexes of the $\boldsymbol{\mu}'(R)$ correspond to the angular momenta of the colliding (or Rydberg) electron.
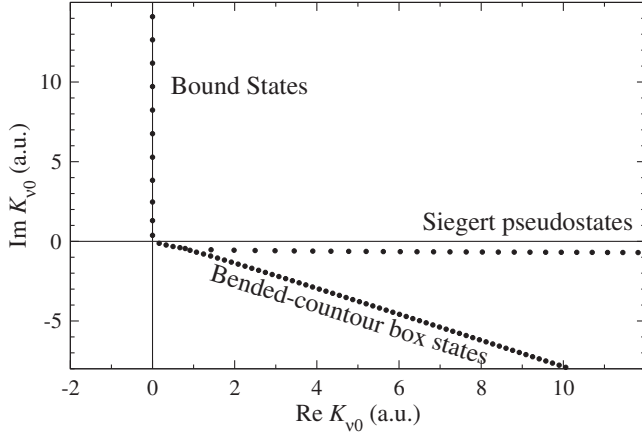
FIG. 3.   Distribution of the ECS poles in the complex momentum plane for $j = 0$. The branch of poles denoted as Siegert pseudostates contains those ECS poles that coincide with the outgoing-wave poles obtained by the Siegert boundary condition [22] set at R_0.

some of the previous DR studies [24–26]. However, in the ECS approach some of the lowest continuum Siegert pseudostates are replaced by a branch of states corresponding to the box states on the rotated coordinate. The desired completeness of the set of states $\phi_{\nu j}$ for the present calculations is reached with 160 states (ordered by the absolute value of the corresponding energy) for each rotational quantum number j.

With the energy-dependent quantum defects (2) and the rovibrational basis $\phi_{\nu j}(Z)$ capable to cover rovibrational excitation and dissociation of the system, all requisite elements needed are now ready to implement the energy-dependent frame transformation procedure. This procedure has been derived in detail and benchmarked against the exact results of the 2D model in Ref. [10]. The resulting initial state-dependent DR cross section can be written as a sum

$$\sigma_{\nu' j'}(E_c) = \frac{1}{2j' + 1} \sum_{\eta J l'} (2J + 1) \sigma_{\nu' j' l'}^{J\eta}(E_c), \qquad (5)$$

where E_c is the collision energy, l' denotes the initial angular momentum of the colliding electron, $\vec{J} = \vec{j'} + \vec{l'}$ is the total angular momentum, and $\eta(-1)^J$ represents the parity of the whole system. The odd η constituents of the cross sections are negligible in this study, as they depend only on the weak $\Lambda = 1, 2$ components of the quantum defects [27]. Nevertheless, our calculations have included them. The initial state-dependent recombination rate is simply

$$\alpha_{\nu' j'}(E_c) = \sqrt{2E_c} \sigma_{\nu' j'}(E_c). \qquad (6)$$

The physical S matrix, from which the cross sections (5) are derived, is a result of the MQDT procedure called the elimination of closed channels:

$$S^{\text{phys}} = S^{oo} - S^{oc}[S^{cc} - e^{-2i\beta(E)}]^{-1}S^{co}, \qquad (7)$$

where the superscripts o and c denote open and closed subblocks in the short-range S matrix, respectively. The diagonal matrix $\beta(E)$ describes effective Rydberg quantum numbers with respect to the closed-channel thresholds E_i:

$$\beta_{ij} = \frac{\pi}{\sqrt{2(E_i - E)}} \delta_{ij}. \qquad (8)$$

The inversed term on the rhs of Eq. (7) generates a series of dense resonances accumulating to each of the closed-channel ionization thresholds. These resonances are associated with the autoionizing and predissociating states of the neutral HeH system. In order to compare our computed DR rates with the most recent experiment, and also for likely future applications of these calculated recombination rates, our raw numerical data must be convolved over the electron energy distributions relevant to any appropriate environment. In astrophysical applications, a Maxwell-Boltzmann distribution of electrons is often assumed [28,29]. In storage-ring experiments, on the other hand, the electron beam exhibits an anisotropic distribution. The velocity parallel to the ion beam is usually well defined with a small spread in the parallel energy ($\Delta E_{||} = 0.1$ meV in Ref. [4]). Divergence of the electron beam is measured by the perpendicular spread, $\Delta E_{\perp} = 2$ meV in Ref. [4]. The details and formulas for the thermal (Maxwell) and anisotropic convolutions can be found in Refs. [30,31].

Figure 4 summarizes our results, along with the recent measurements at CSR [4], for different initial rotational states j' (the initial vibrational state is always $\nu' = 0$). The red curve represents the calculated DR rate convolved over the anisotropic electron beam distributions. The black curve shows the DR rate with the toroidal correction [32,33] applied to the computed data. The toroidal correction accounts for the collisional events that happen in the bending areas where the two beams merge or diverge. In these areas the relative collisional energy is higher. Such events effectively increase the energy spread, well beyond the values of $\Delta E_{||}$ and $\Delta E_{\perp}$, for a fraction of the DR events. The black circles with error bars denote the data measured recently at the CSR [4].

The present calculations clearly confirm the experimentally observed [4] low-energy behavior of the DR rate for the cold HeH$^+$ ions. The introduction of energy-dependent body-frame quantum defects into the theory has shifted some low-energy closed-channel resonances, resulting in low-energy DR rates that differ from the results of previous theoretical studies, and this appears to produce improved agreement with experiment. In particular, the steep increase of the DR rate for $j' = 0$ at zero energy (Fig. 13 in Ref. [9]) was caused by a $l = 1$ closed-channel resonance positioned at 1 meV. The energy dependence of $\mu(R)$ shown in Fig. 2 causes this resonance to move to the negative collision energies, making it a bound Rydberg state of the neutral HeH that no longer affects the computed DR rate.

We have also attempted to estimate the sensitivity of the computed rates to the accuracy of the electronic-structure
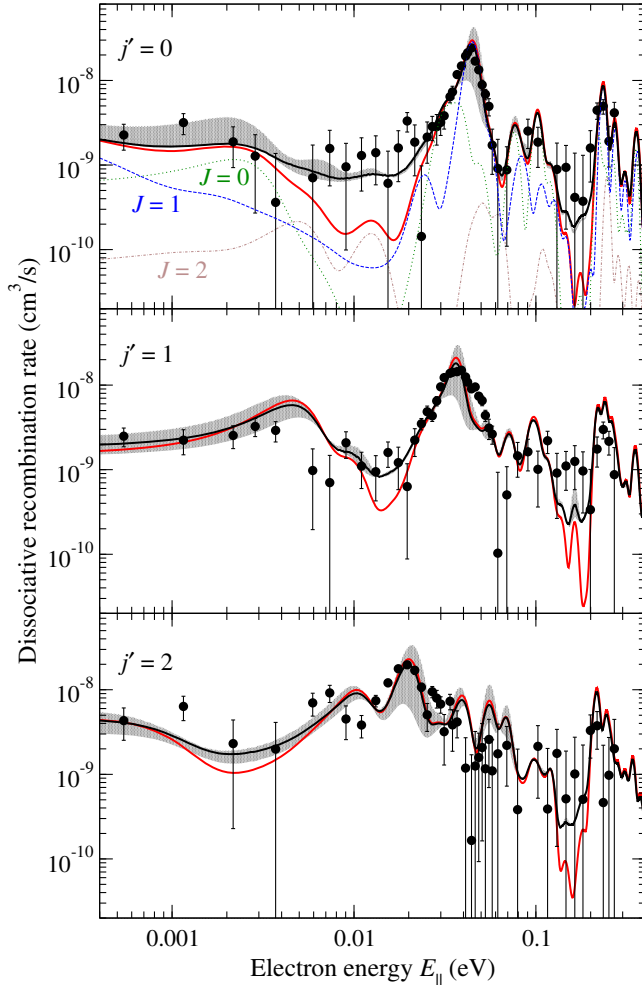
FIG. 4. Shown here is the DR rate anisotropically averaged with $\Delta E_{\parallel} = 0.1$ meV and $\Delta E_{\perp} = 2$ meV. The initial vibrational state is $\nu' = 0$ and the initial rotational state changes from $j' = 0$ (top panel) to $j' = 2$ (bottom panel). The red curve shows the present calculations without toroidal effects included, while the black curve accounts for the toroidal correction [32]. The shaded area estimates the uncertainty of our calculations (see more details in the text). The black circles with error bars display DR rates measured at the CSR [4]. The top panel also shows the decomposition of the computed DR rate into channels with different total angular momenta J (dashed lines).

FIG. 5. Plasma rate coefficients are shown for different initial rotational states $j' = 0$, 1, 2. The solid curves result from the present theory, while the dashed curves are taken from the experiment at the CSR [4]. The dot-dashed line represents data employed by Guesten *et al.* [1] in their chemistry kinetics simulations of NGC 7027.

calculations. To this extent a random noise matrix $\Delta\boldsymbol{\mu}$ of the maximum value of $\delta = 0.002$ was added to and subtracted from the original $\boldsymbol{\mu}^{\Lambda}(R, \epsilon)$ in Eq. (2). The value of δ reflects our observations of variations of $\boldsymbol{\mu}^{\Lambda}(R, \epsilon)$ due to the electronic basis set size and due to the extent of the space of configuration interaction. The resulting variations of the computed DR rates are shown as a shaded area in Fig. 4. One observes that the low-energy region is more sensitive to the accuracy of the quantum defects. We observe 30%–50% variations of the DR rate below 1 meV and changes by a multiplicative factor of 2–3 in the area of the peak (20–45 meV, depending on the j'). At higher energies these
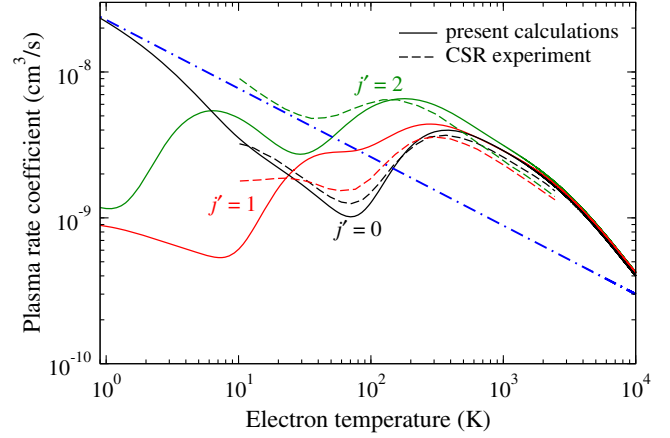
variations appear to be smeared out by the broader effective electron energy distribution.

A last bit of information shown in the top panel of Fig. 4 is the decomposition of the computed DR rate into channels with different total angular momentum J in a manner similar to Eq. (5). However, all the angular factors are included in the presented data, so the red curve is just a direct sum of the $J = 0$, 1, 2 curves. It is clear that the peak at 45 meV is created dominantly in the $J = 1$ channel which is in agreement with the experimentally observed angular distribution of fragments [4] formed by the rotational $j = 1$ angular shape.

Plasma rate coefficients are obtained by an average of the state-specific DR rate over the Maxwellian distribution of the colliding electrons. The computed plasma rates are shown in Fig. 5 for the lowest initial rotational states $j' = 0$, 1, 2. The $j' = 0$ results compare very well with the plasma rate coefficients derived from the CSR experiment [4]. Agreement between the theory and the experiment is poorer for the initial states $j' = 1$ and $j' = 2$. These discrepancies for $j' = 1$, 2 visible below 100 K can be linked with the discrepancies seen in Fig. 4 below 10 meV.

The dot-dashed line represents the temperature dependence of the plasma rate coefficient employed in the temperature and density simulations of NGC 7027 [1]. These simulations were carried out to estimate the emissivity of the $j = 1 \to 0$ line of HeH$^+$ ions [having the functional form: $k_2 = 3.0 \times 10^{-10}(T/10^4)^{-0.47}$ cm^3/s]. Our present calculations estimate the plasma rate coefficient at 10^4 K to be slightly above 4.0×10^{-10} cm^3/s. These results therefore suggest that the unexpectedly high brightness of the $j = 1 \to 0$ transition observed in the first HeH$^+$ detection is not caused by the slower destruction of the HeH$^+$ cations via the DR process.

The energy-dependent FT [10] was applied in the present study for a case controlled by the indirect DR mechanism. Molecular systems with an additional direct mechanism exhibit much stronger negative-energy dependence of quantum defects, thus providing a more stringent test of the theory. The applicability of the present theory for systems with the direct mechanism still remains to be seen. A corresponding direct DR study for H_2^+ is under way.

---

*roman.curik@jh-inst.cas.cz

[1] R. Guesten, H. Wiesemeyer, D. Neufeld, K. M. Menten, U. U. Graf, K. Jacobs, B. Klein, O. Ricken, C. Risacher, and J. Stutzki, Nature (London) **568**, 357 (2019).

[2] S. Vranckx, J. Loreau, M. Desouter-Lecomte, and N. Vaeck, J. Phys. B **46**, 155201 (2013).

[3] C. Stromholm, J. Semaniak, S. Rosen, H. Danared, S. Datz, W. van der Zande, and M. Larsson, Phys. Rev. A **54**, 3086 (1996).

[4] O. Novotny, P. Wilhelm, D. Paul, A. Kalosi, S. Saurabh, A. Becker, K. Blaum, S. George, J. Goeck, M. Grieser et al., Science **365**, 676 (2019).

[5] S. L. Guberman, Phys. Rev. A **49**, R4277 (1994).

[6] H. Takagi, Phys. Rev. A **70**, 022709 (2004).

[7] H. Takagi and M. Tashiro, EPJ Web Conf. **84**, 02002 (2015).

[8] D. J. Haxton and C. H. Greene, Phys. Rev. A **79**, 022701 (2009); **84**, 039903(E) (2011).

[9] R. Čurík and C. H. Greene, J. Chem. Phys. **147**, 054307 (2017).

[10] D. Hvizdoš, R. Čurík, and C. H. Greene, companion paper, Phys. Rev. A **101**, 012709 (2020).

[11] R. Čurík, D. Hvizdoš, and C. H. Greene, Phys. Rev. A **98**, 062706 (2018).

[12] See Supplemental Material at http://link.aps.org/supplemental/10.1103/PhysRevLett.124.043401 containing detailed unconvolved DR rates together with the elaborated energy dependence of the quantum defects. The Supplemental Material includes Refs. [13–16].

[13] MOLPRO, version 2010.1, a package of ab initio programs, H.-J. Werner, P. J. Knowles, G. Knizia, F. R. Manby, M. Schütz, and others, see http://www.molpro.net.

[14] T. H. Dunning, J. Chem. Phys. **90**, 1007 (1989).

[15] A. Petrignani, S. Altevogt, M. H. Berg, D. Bing, M. Grieser, J. Hoffmann, B. Jordon-Thaden, C. Krantz, M. B. Mendes, O. Novotný et al., Phys. Rev. A **83**, 032711 (2011).

[16] F. O. Waffeu Tamo, H. Buhr, O. Motapon, S. Altevogt, V. M. Andrianarijaona, M. Grieser, L. Lammich, M. Lestinsky, M. Motsch, I. Nevo et al., Phys. Rev. A **84**, 022710 (2011).

[17] L. A. Morgan, C. J. Gillan, J. Tennyson, and X. S. Chen, J. Phys. B **30**, 4087 (1997).

[18] I. Ema, J. M. G. D. la Vega, G. Ramirez, R. Lopez, J. F. Rico, H. Meissner, and J. Paldus, J. Comput. Chem. **24**, 859 (2003).

[19] J. A. Coxon and P. G. Hajigeorgiou, J. Mol. Spectrosc. **193**, 306 (1999).

[20] B. Simon, Phys. Lett. A **71**, 211 (1979).

[21] C. W. McCurdy and F. Martín, J. Phys. B **37**, 917 (2004).

[22] O. I. Tolstikhin, V. N. Ostrovsky, and H. Nakamura, Phys. Rev. A **58**, 2077 (1998).

[23] A. J. F. Siegert, Phys. Rev. **56**, 750 (1939).

[24] E. L. Hamilton and C. H. Greene, Phys. Rev. Lett. **89**, 263003 (2002).

[25] R. Čurík and C. H. Greene, Phys. Rev. Lett. **98**, 173201 (2007).

[26] R. Čurík and F. A. Gianturco, Phys. Rev. A **87**, 012705 (2013).

[27] E. S. Chang and U. Fano, Phys. Rev. A **6**, 173 (1972).

[28] L. H. Andersen and J. Bolko, Phys. Rev. A **42**, 1184 (1990).

[29] S. Lepp, P. C. Stancil, and A. Dalgarno, J. Phys. B **35**, R57 (2002).

[30] V. Kokoouline and C. H. Greene, Phys. Rev. A **68**, 012703 (2003).

[31] R. Čurík and C. H. Greene, Mol. Phys. **105**, 1565 (2007).

[32] O. Novotný, A. Becker, H. Buhr, C. Domesle, W. Geppert, M. Grieser, C. Krantz, H. Kreckel, R. Repnow, D. Schwalm et al., Astrophys. J. **777**, 54 (2013).

[33] V. Kokoouline and C. H. Greene, Phys. Rev. A **72**, 022712 (2005).